MOLECULAR AND CELLULAR BIOLOGY, Feb. 2003, p. 1304–1315 Vol. 23, No. 4
0270-7306/03/$08.00+0 DOI: 10.1128/MCB.23.4.1304–1315.2003

Mouse Germ Cell-Less as an Essential Component for Nuclear Integrity

Tohru Kimura,[1] Chizuru Ito,[2] Shoko Watanabe,[1] Tohru Takahashi,[3] Masahito Ikawa,[4] Kentaro Yomogida,[5] Yukiko Fujita,[1] Megumi Ikeuchi,[1] Noriko Asada,[1] Kiyomi Matsumiya,[3] Akihiko Okuyama,[3] Masaru Okabe,[4] Kiyotaka Toshimori,[2] and Toru Nakano[1]*

Department of Molecular Cell Biology[1] and Department of Laboratory Sciences for Animal Experimentation,[5] Research Institute for Microbial Diseases, Osaka University, Suita-shi, Osaka 565-0871, Department of Anatomy and Reproductive Cell Biology, Miyazaki Medical College, Kiyotake, Miyazaki 889-1692,[2] Department of Urology, Osaka University Medical School, Suita-shi, Osaka 565-0871,[3] and Genome Information Research Center, Osaka University, Suita-shi, Osaka 565-0871,[4] Japan

Received 19 September 2002/Returned for modification 16 October 2002/Accepted 18 November 2002

A mouse homologue of the *Drosophila melanogaster germ cell-less* (*mgcl-1*) gene is expressed ubiquitously, and its gene product is localized to the nuclear envelope based on its binding to LAP2β (lamina-associated polypeptide 2β). To elucidate the role of *mgcl-1*, we analyzed two mutant mouse lines that lacked *mgcl-1* gene expression. Abnormal nuclear morphologies that were probably due to impaired nuclear envelope integrity were observed in the liver, exocrine pancreas, and testis. In particular, functional abnormalities were observed in testis in which the highest expression of *mgcl-1* was detected. Fertility was significantly impaired in *mgcl-1*-null male mice, probably as a result of severe morphological abnormalities in the sperm. Electron microscopic observations showed insufficient chromatin condensation and abnormal acrosome structures in *mgcl-1*-null sperm. In addition, the expression patterns of transition proteins and protamines, both of which are essential for chromatin remodeling during spermatogenesis, were aberrant. Considering that the first abnormality during the process of spermatogenesis was abnormal nuclear envelope structure in spermatocytes, the *mgcl-1* gene product appears to be essential for appropriate nuclear-lamina organization, which in turn is essential for normal sperm morphogenesis and chromatin remodeling.

The physiological functions of numerous genes, including transcription factors and signaling molecules, are reportedly conserved in *Drosophila melanogaster* and mammals. However, by and large, the functional mammalian homologues of the germ cell-specifying genes in *Drosophila* have not been established, partially because the molecular mechanisms of germ cell specification in mammals are quite different from those in *Drosophila* (45). One of the major reasons for this is that *Drosophila* has a determinant of germ cell formation in the egg cytoplasm, i.e., the germ plasm, which is not present in mammals.

The *Drosophila germ cell-less* (*gcl*) gene product (GCL) is a component of the germ plasm and is a critical factor for primordial germ cell (PGC) formation (24, 25, 32). Recently, we and another group identified a mouse homologue of *gcl*, named *mouse germ cell-less-1* (*mgcl-1*) (27, 29). The *mgcl-1* gene product (mGCL-1) had 36% identity and 56% similarity with the *Drosophila* GCL, and both the *Drosophila* and mouse *gcl* gene products contained the BTB/POZ domain, which is a conserved protein-protein interaction domain (7). Although genetic analysis clearly revealed that *mgcl-1* could rescue the *Drosophila gcl* mutation, the molecular mechanism whereby GCL regulates germ lineage determination has not been elucidated. Northern blotting and RNase protection assays have shown that *mgcl-1* is expressed ubiquitously, with the highest levels of expression occurring during spermatogenesis. Nevertheless, the in vivo function of mGCL-1 remains elusive.

The *mglc-1* gene was cloned independently by two research groups using two-hybrid analysis. One group identified mGCL-1 as DIP (DP-interacting protein), which is a protein that interacts with the DP component of E2F (14). E2F, which is an important transcription factor for the orchestration of early cell cycle progression, plays its role when it forms a heterodimer with DP (28). DIP/mGCL-1 was located in the nuclear envelope, wherein it formed a speckled pattern and showed a dominant influence on the distribution of DP proteins. The overexpression of DIP/mGCL-1 not only reduced the transcriptional activity of the E2F-DP heterodimer but also induced cell cycle arrest at the G_1 phase, which was modulated by the expression of DP proteins. Thus, one possible role for mGCL-1 is as a cell cycle regulator via interaction with the E2F-DP heterodimer.

The second research group identified mGCL-1 as a LAP2β (lamina-associated polypeptide 2β)-binding protein (31). LAP2β has been isolated and characterized as an integral inner nuclear membrane protein that binds lamin B and chromosomes in a phosphorylation-dependent manner (15). The mGCL-1 protein bound to LAP2β and was colocalized with LAP2β to the nuclear envelope, the region in which the *Dro-*

* Corresponding author. Mailing address: Department of Molecular Cell Biology, Research Institute for Microbial Diseases, Osaka University, 3-1 Yamada-oka, Suita, Osaka 565-0871, Japan. Phone: 81-6-6879-8361. Fax: 81-6-6879-8362. E-mail: tnakano@biken.osaka-u.ac.jp.

sophila GCL is also located (24). Nuclear fractionation studies have revealed that mGCL-1 is a nuclear matrix component, but it is not an integral protein of the nuclear envelope. Transcription assays have revealed that LAP2β has the capacity to interfere with the transcriptional activity of the E2F-DP complex, and this interference is more potent than that induced by mGCL-1. In addition, coexpression of mGCL-1 and LAP2β has synergistic effects on the inhibition of E2F-DP-induced transcriptional activation.

In order to elucidate the in vivo function of *mgcl-1*, we analyzed two lines of mGCL-1-null mice. The mGCL-1-null embryonic fibroblasts did not manifest significant cell cycle aberrations. However, the nuclear morphologies of cells in the liver, exocrine pancreas, and testis were abnormal. Consistent with the high mGCL-1 expression in testis, the male mutant mice showed abnormal spermatogenesis, impaired fertility, and aberrant chromatin remodeling during spermatogenesis. We consider mGCL-1-null mice to provide new insights into the function of nuclear envelope integrity and chromatin remodeling.

MATERIALS AND METHODS

Production of *mgcl-1*-null mice. Mouse 129Sv/J genomic clones that contain the *mgcl-1* gene have been described previously (27). The 2.9-kb *Spe*I-*Bam*HI fragment that encompasses exon 2 was replaced with a neomycin resistance cassette in the pPNT vector (40). A 5.3-kb *Eco*RI-*Spe*I fragment was inserted between the neomycin resistance cassette and the herpes simplex virus thymidine kinase gene, both of which are driven by the *PGK1* promoter. A 1.5-kb *Bam*HI-*Pst*I fragment was inserted upstream of the neomycin resistance gene. The resulting targeting vector, pKO-GCL-4, was electroporated into D3 embryonic stem (ES) cells and selected with G418 and ganciclovir. Targeting events were screened by PCR and confirmed by Southern blot analysis using digestion with several restriction enzymes and both 3′- and 5′-end probes. The recombinant cells were karyotyped to ensure that 2*N* chromosomes were present in the majority of the metaphase spreads. Chimeric mice, which were derived from correctly targeted ES cells, were mated to C57BL/6 mice to obtain F_1 *mgcl-1*$^{+/-}$ mice. The mouse strain with the retrovirus insertion at the *mgcl-1* locus was derived from the OST6847 ES cell line (Lexicon Genetics, The Woodlands, Tex.) (48).

Anti-mGCl-1 antibodies and Western blot analysis. To generate the anti-mGCL-1 antibody, a glutathione *S*-transferase fusion protein was produced in bacteria. The 630-bp *Sma*I-*Xho*I fragment of *mgcl-1* cDNA was cloned into the *Sma*I-*Xho*I site of the bacterial expression vector pGEX4T-2 (Amersham Pharmacia, Little Chalfont, Buckinghamshire, United Kingdom). The expression of the fusion protein was induced by the addition of 0.1 mM IPTG (isopropyl-β-D-thiogalactopyranoside) for 3 h, and the protein was purified by absorption onto glutathione agarose beads, according to the manufacturer's recommendation. The purity of the recombinant protein was assessed on sodium dodecyl sulfate (SDS)-polyacrylamide gels by staining with Coomassie brilliant blue. Polyclonal antibodies were raised by injecting approximately 2 mg of purified protein into a rabbit, with repeat injections 3, 6, and 9 weeks later. The glutathione *S*-transferase–mGCL-1 fusion protein was used in the affinity purification of polyclonal anti-PGC7 antibodies. The antibody was used at a 1:500 dilution.

The testes were homogenized in a solution of 150 mM NaCl, 1% Nonidet P-40, 0.5% sodium deoxycholate, 0.1% SDS, and 50 mM Tris-HCl (pH 8.0) that contained protease inhibitors. The mGCL-1 protein partitioned into the insoluble fraction. The insoluble material was dissolved in SDS-polyacrylamide gel electrophoresis sample buffer, resolved on an SDS–10% polyacrylamide gel, and transferred to a polyvinylidene difluoride membrane (Millipore, Bedford, Mass.). The filters were blocked overnight with 2% nonfat dry milk in 20 mM Tris–150 mM NaCl–0.05% Tween 20 and then incubated with the anti-mGCL-1 antibody. The secondary antibody was goat anti-rabbit immunoglobulin G (IgG) conjugated to peroxidase (Zymed, San Francisco, Calif.), which was diluted at 1:2,000. Signals were detected using the ECL Western blotting detection reagents (Amersham Pharmacia). The soluble fraction was also analyzed, but mGCL-1 was not detected in either the wild-type or *mgcl-1*-null testes (data not shown).

Isolation and growth of MEFs. Mouse embryonic fibroblasts (MEFs) were prepared from day-13.5 embryos, and grown in Dulbecco's modified Eagle medium that was supplemented with 10% fetal bovine serum. Serial cell culturing was carried out according to the 3T3 protocol (39). Briefly, 3×10^5 cells were plated on a 6-cm-diameter dish; the cells were counted 3 days later, and 3×10^5 cells were replated. The growth rate at each time point was calculated by dividing the final number of cells by the initial number of cells.

Northern blots and semiquantitative RT-PCR analyses. Total RNA was extracted from MEFs and testes using the RNeasy mini kit (Qiagen, Valencia, Calif.). Northern blot analysis was carried out as described previously (26). In brief, 10 μg of total RNA was separated on a 1% agarose gel that contained 2.1 M formaldehyde and blotted onto Hybond N+ filters (Amersham Pharmacia). The filters were UV cross-linked at 150 mJ. The filters were then hybridized with radiolabeled probes in 0.5 M $NaPO_4$ (pH 7.2)–7% SDS–0.5 mM EDTA at 65°C for 15 h. The filters were washed twice for 10 min at room temperature and once for 30 min at 65°C with 0.04 M $NaPO_4$ that contained 1% SDS. The filters were exposed to a Fuji imaging plate and analyzed on a BAS2000 system (Fuji Photo Co., Tokyo, Japan). The probes were isolated by reverse transcription (RT)-PCR with testis RNA as the template. The amplified probes were cloned into the pCR2.1 vector (Invitrogen, Carlsbad, Calif.), and the sequences were confirmed using the Big Dye terminator kit with ABI PRISM 310 and 377 automated DNA sequencers (PE Applied Biosystems, Foster City, Calif.). The probes were labeled with [α-^{32}P]dCTP (ICN, Costa Mesa, Calif.) using the BcaBest DNA labeling kit (Takara, Tokyo, Japan).

For semiquantitative RT-PCR, 1 μg of total RNA was reverse transcribed with the ThermoScript RT-PCR System (Invitrogen). Semiquantitative PCR was performed for 1 cycle at 95°C for 1 min, followed by amplification cycles of 95°C for 30 s, 60°C for 30 s, 72°C for 40 s, and finally 72°C for 7 min, in a PCR system 9700 (PE Applied Biosystems). PCR amplification of the cDNA remained linear for 30 cycles (data not shown). The amplification cycles for each gene were as follows: *cyclin A*, 27 cycles; *cdc2*, 25 cycles; *DNA polymerase* α, 27 cycles; and β-*actin*, 25 cycles. The PCR products were analyzed by 2.0% agarose gel electrophoresis, and visualized using ethidium bromide staining.

The following primer pairs were used for PCR amplification: *Rb*, 5′-CATCG TCACTGCCTACAAGG-3′ and 5′-GAGGTCCTCACTTTTCCTCC-3′; *p107*, 5′-ATGCCACAAAGACTCCCAAC-3′ and 5′-TGCTTTGATCAGGCAAAG GG-3′; *E2F1*, 5′-CCTCGCAGATCGTCATCATC-3′ and 5′-GCAGCTCCAAG AAGCGTTTG-3′; *cyclin E*, 5′-ACCTGCCATTGCCTCCAAAG-3′ and 5′-GAAGGCAGGACATGCTGTTG-3′; *cdc2*, 5′-GCAGTTCATGGATTCTTCA C-3′ and 5′-CCGTTCTCGTCCAGGTTCTT-3′; *DNA polymerase* α, 5′-CACC GTTGACCTTCATGGTACA-3′ and 5′-TGTACCGGTAAAAGCACAGCTG-3′; β-*actin*, 5′-GTGACGAGGCCCAGAGCAAGAG-3′ and 5′-AGGGGCCGG ACTCATCGTACTC-3′; *Prm1*, 5′-ATGGCCAGATACCGATGCTG-3′ and 5′-CTAGTATTTTTTACACCTTATGG-3′; *Prm2*, 5′-ATGGTTCGCTACCGAA TGAG-3′ and 5′-TTAGTGATGGTGCCTCCTAC-3′; *TP1*, 5′-ATGTCGACC AGCCGCAAGC-3′ and 5′-TCACAAGTGGGATCGGTAATTG-3′; *TP2*, 5′-A TGGACACCAAGATGCAGAG-3′ and 5′-TCACTTGTATCTTCGCCCTG-3′; *Tarbp2*, 5′-ATGAGTGAAGAGGATCAGGG-3′ and 5′-CTACTTGCTACC CGCCATG-3′; *Camk4*, 5′-CAAGATGCCAAGGACAGCAC-3′ and 5′-TTAG TACTCTGGCTGAATCG-3′; *Csnk2a2*, 5′-CAACATTCACGGAAGCGCTG-3′ and 5′-GCTTATGGAAAAGTGGGAG-3′.

Histology and immunohistochemistry. For the standard histological analysis, the tissues were fixed with 4% paraformaldehyde or Carnoy's solution and embedded in methyl methacrylate. The sections were stained with hematoxylin or hematoxylin and eosin (HE).

For the immunohistochemistry of nuclear envelope proteins, the tissues were fixed with 4% paraformaldehyde, embedded in OCT compound (Tissue-Tek, Elkhart, Ind.), and frozen in dry ice. The sections were cut at a thickness of 7 μm in a CM3050 cryostat (Leica, Nußloch, Germany) and melted onto aminopropyltriethoxy silane-coated slides. The slides were treated with 0.2% Triton X-100 in PBS and then blocked for 1 h with 2% normal goat serum or 3% bovine serum albumin in phosphate-buffered saline, followed by overnight incubation in the primary antibodies. The following day, signals were detected by incubating the slides in the secondary antibodies for 1 h. Propidium iodide was utilized for nuclear staining. The primary antibodies (and dilutions thereof) were anti-lamin-B goat serum (M20, 1:40; Santa Cruz Biotechnology, Santa Cruz, Calif.), anti-LAP2 (monoclonal antibody [MAb] clone 27, 1:500; Transduction Laboratories, Lexington, Ky.), and anti-NPC (MAb 414, 1:500; DabCO, Richmond, Calif.). The slides were analyzed using an LSM510 confocal laser scanning microscope (Carl Zeiss, Jena, Germany). The Alexa488-conjugated anti-goat-Ig(H+L) antibody and the anti-mouse-Ig(H+L) antibody (used at 1:200 dilutions) were purchased from Molecular Probes (Eugene, Oreg.).

For the immunohistochemistry of sperm basic proteins, the testes were fixed

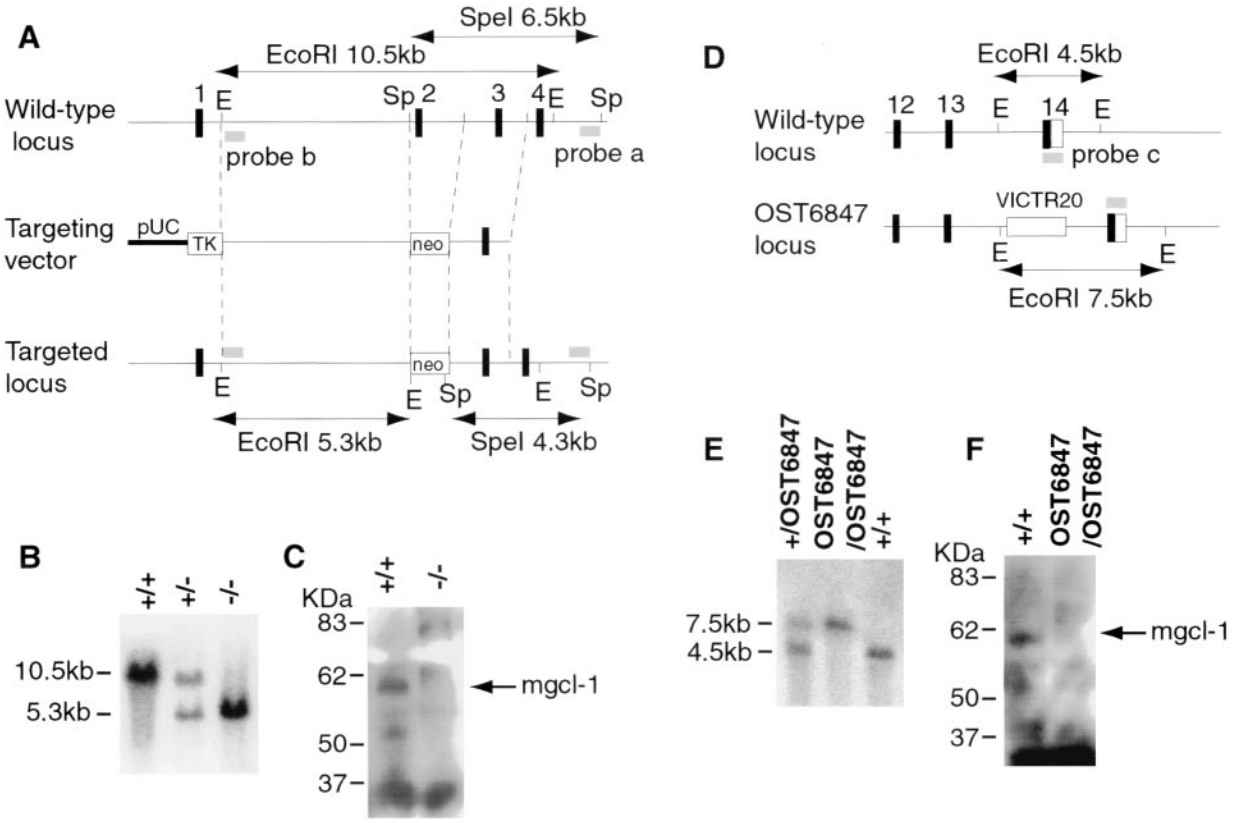

FIG. 1. Two *mgcl-1*-null mice. The left and right panels show the respective data for *mgcl-1*$^{-/-}$ mice that were produced by homologous recombination and for *mgcl-1*$^{OST6847/OST6847}$ mice that were produced by retroviral insertional mutagenesis. (A and D) Maps of the wild-type *mgcl-1* locus, targeting vector, and disrupted loci. The diagnostic restriction enzyme digestion patterns are indicated. Abbreviations: E, *Eco*RI; Sp, *Spe*I. (B and E) Southern blot analysis. The genomic DNA from each genotype was digested with *Eco*RI and hybridized with the 3′-terminal probes b (B) and c (E). (C and F) Western blot analysis. Extracts from the testes were separated on SDS-polyacrylamide gels and analyzed with an affinity-purified, anti-mGCL-1 polyclonal antibody.

with Carnoy's solution and embedded in methyl methacrylate. The sections were cut at a thickness of 5 μm and rehydrated. Antigen retrieval was conducted by boiling the slides in 10 mM tri-sodium citrate (pH 6.0) for 20 min. After blocking with 10% normal goat serum in phosphate-buffered saline that contained 0.1% Triton X-100, the slides were incubated with the primary antibodies. The following day, the slides were incubated with either biotin-conjugated anti-mouse-Ig(H+L) antibody (1:200; Vector Lab, Burlingame, Calif.) or an anti-rabbit-Ig(H+L) antibody (1:400; Vector Lab) for 1 h, followed by incubation with streptavidin-horseradish peroxidase (1:100; Invitrogen) for 1 h. The mouse MAbs against protamine 1 and 2, Hup1N (1:100) and Hup2B (1:100), were kindly gifted by R. Balhorn, Lawrence Livermore National Laboratory (37). The rabbit polyclonal anti-transition protein 1 (1:100) and 2 (1:100) antibodies were gifted by S. Kestler, University of South Carolina (2, 22). Finally, the sections were counterstained with either periodic acid-Schiff-hematoxylin or methylgreen.

Analysis of sperm and sperm protamines. Sperm samples were collected from the cauda epididymides of adult male mice that were 2 to 6 months of age, dried on aminopropyltriethoxy silane-coated slides, and stained with HE. Sperm morphology was classified a posteriori into four groups, as described in the text below. At least 200 sperm were analyzed per individual mouse. Sperm motility was estimated using HTM-IVOS (version 10) according to the manufacturer's recommendation (Hamilton-Thorn Research, Danvers, Mass.). The methods for protamine (Prm) extraction, acid urea polyacrylamide gel electrophoresis, and Western blot analysis have been described elsewhere (6). Briefly, the sperm samples were suspended in 50 mM Tris-HCl (pH 8.0) and 10 mM dithiothreitol using sonication and incubated at 4°C for 15 min. After the sperm tails were dissolved by treatment with 1% CTAB (cetyltrimethylammonium bromide), the sperm heads were purified by centrifugation and counted. Protamines were purified by standard procedures and dissolved at a concentration of 10^8 sperm heads/ml in 0.9 M acetate–0.5 M 2-mercaptoethanol–20% sucrose. The proteins were then subjected to 15% acid urea polyacrylamide gel electrophoresis. For Western blot analysis, the proteins were transferred onto a nitrocellulose membrane (Schleicher & Schuell, Dassel, Germany) using wet electrophoretic transfer in 0.9% acetate. Western blot analysis was carried out as described above. The mouse MAbs Hup1N (1:200) and Hup2B (1:200) were used to identify Prm-1 and Prm-2, respectively (37). A peroxidase-conjugated goat anti-mouse IgG antibody (Zymed) was diluted 1:1,000 and used as the secondary antibody.

Electron microscopy. Testes were fixed with 2.5% glutaraldehyde and 2% osmium tetroxide, and small pieces of the testes were routinely dehydrated and embedded in Epon 812 to make thin sections. The sections were double stained with uranium acetate and lead citrate and then examined using transmission electron microscopy at an accelerating voltage of 75 kV (H7100-type transmission electron microscope; Hitachi, Tokyo, Japan). The negative films and the images were digitized and processed using Adobe Photoshop 6 (Adobe Systems Inc., Mountain View, Calif.) and printed with a Pictrostat Digital 400 printer (Fuji Film, Tokyo, Japan).

RESULTS

Normal cell growth and expression of E2F-DP target genes in *mgcl-1*-null embryonic fibroblasts. Two *mgcl-1*-null mice were produced and analyzed in this study. In the first murine line, *mgcl-1* expression was disrupted by the deletion of exon 2 via homologous recombination in ES cells (Fig. 1A). Targeted ES cell lines were transferred into germ lines, and the subsequent F1 *mgcl-1*$^{+/-}$ crosses produced *mgcl-1*$^{-/-}$ mice in Men-

delian ratios (Fig. 1B). Expression of the mGCL-1 protein was not detected in the *mgcl-1*$^{-/-}$ mice (Fig. 1C). The second *mgcl-1*-deficient mouse strain (*mgcl-1*^{OST6847}) was derived from an ES cell line in which a retrovirus vector was inserted into the *mgcl-1* locus (Fig. 1D and E) (48). Neither the full-length nor the truncated mGCL-1 protein was detected in the homozygous *mgcl-1*$^{OST6847/OST6847}$ strains (Fig. 1F). Since the *mgcl-1*$^{OST6847/OST6847}$ mice exhibited essentially the same phenotype as the *mgcl-1*$^{-/-}$ mice, the following results are derived mainly from the *mgcl-1*$^{-/-}$ mice.

Previous reports showed that mGCL-1 overexpression induced cell cycle arrest and reduced E2F-dependent transactivation (14, 31). First, we compared the cell growth and gene expression characteristics of E2F-dependent genes among *mgcl-1*$^{+/+}$, *mgcl-1*$^{+/-}$, and *mgcl-1*$^{-/-}$ embryonic fibroblasts (Fig. 2). There were no significant differences in the growth curves of primary embryonic fibroblasts (Fig. 2A) and the growth rate of embryonic fibroblasts when they were passed every 3 days (Fig. 2B). The promoters of various genes, which included those for the cell cycle regulators Rb, p107, cyclin A, and p34^{cdc2}, are driven by the E2F-DP complexes (28). The mRNA levels of the genes for Rb, p107, E2F1, cyclin E, cyclin A, p34^{cdc2}, and DNA polymerase α, all of which have been reported to be activated by E2F-DP1, were analyzed by Northern blotting or RT-PCR analyses. The embryonic fibroblasts and testes showed no significant differences with respect to gene expression in either the control (*mgcl-1*$^{+/+}$ or *mgcl-1*$^{+/-}$) or *mgcl-1*$^{-/-}$ genetic backgrounds.

Abnormal nuclear morphology in cells of the liver, exocrine pancreas, and testis. In addition to binding to the DP component of E2F-DP, mGCL-1 was reported to bind to LAP2β (31). These data encouraged us to analyze the nuclear morphologies of various organs of the *mgcl-1*-null mice. Hematoxylin staining and immunohistochemical staining with anti-nuclear pore complex (anti-NPC), anti-lamin B, and anti-LAP2 antibodies showed that cells in the liver, exocrine pancreas, and testis had abnormal nuclear structures (Fig. 3 and 4). Compared to the circular or ovoid-shaped nuclei in the liver and exocrine pancreas of control mice, the vast majority of the cells in *mgcl-1*$^{-/-}$ mice exhibited irregularly shaped nuclei (Fig. 3). However, no functional abnormalities were observed in either the liver or exocrine pancreas. The serum concentrations of total protein, albumin, and of enzymes, such as GOT and GPT, were normal in the *mgcl-1*$^{-/-}$ mice (data not shown). As for the function of the exocrine pancreas, the serum pancreatic amylase concentration was normal and a fat-rich diet intake did not cause increased levels of fat in the feces of *mgcl-1*$^{-/-}$ mice (data not shown).

The *mgcl-1* gene is highly expressed in pachytene stage spermatocytes, and its product is localized at the nuclear lamina (27, 29, 31). Irregularly shaped nuclei with deep invaginations of the cytoplasm were observed in the pachytene and diplotene spermatocytes of the *mgcl-1*$^{-/-}$ mice (Fig. 4A). Furthermore, NPC was distributed at constant intervals in the wild-type nuclear envelopes, whereas distribution was irregular and NPC often accumulated at the bottom of invaginated nuclear envelopes in *mgcl-1*$^{-/-}$ mice. These abnormal nuclear structures were confirmed by electron microscopic analysis (Fig. 4B). Thus, both the nuclear structure and the distribution of nuclear envelope components of spermatocytes are perturbed by the null mutation in *mgcl-1*.

Morphological and functional abnormalities of *mgcl-1*-null sperm. The fertility of *mgcl-1*$^{-/-}$ males was reduced significantly, despite an apparent lack of effect on either mating behavior or copulatory plug formation. Significantly fewer homozygous than heterozygous mice were able to sire offspring (6 of 14 versus 14 of 14, respectively; Fisher's exact test, $P < 0.001$). Furthermore, the average litter size of fertile *mgcl-1*$^{-/-}$ males was significantly smaller than that of *mgcl-1*$^{+/-}$ males (4.5 ± 1.9, $n = 14$, and 7.9 ± 2.0, $n = 23$, respectively [mean ± standard deviation]; $P < 0.0001$ by Student's t test). In contrast, neither histological abnormality nor abnormal fertility was observed in *mgcl-1*$^{-/-}$ females (data not shown).

The weights of the testes, cauda epididymides, and seminal vesicles of *mgcl-1*$^{-/-}$ males did not differ between wild-type and *mgcl-1*$^{+/-}$ males (data not shown). However, the number of sperm in the cauda epididymides of *mgcl-1*$^{-/-}$ males ($14.7 \times 10^6 \pm 2.2 \times 10^6$ [mean ± standard error of the mean], $n = 13$) was slightly lower than in those of control males ($27.3 \times 10^6 \pm 3.0 \times 10^6$ [mean ± standard error of the mean], $n = 12$) ($P < 0.005$ by Student's t test). In addition, approximately 60% of the sperm of *mgcl-1*$^{-/-}$ mice had abnormal head morphogenesis (Fig. 5A). Frequently observed abnormalities included blunt acrosomes, ectopic attachment of the flagellum, round heads, or narrowed heads (Fig. 5B; from left to right in the −/− panel). In addition, insufficient chromatin condensation and abnormal acrosome structures were confirmed by electron microscopy (Fig. 5C). Furthermore, sperm that lacked flagella appeared more frequently in *mgcl-1*$^{-/-}$ mice. Finally, the most striking and peculiar abnormality was the appearance in these mice of gigantic sperm with multiple heads and flagella. Several sperm heads were embedded within a large cytoplasm that bundled up the flagella (Fig. 5D to F). This morphological abnormality suggests that defects in the separation of nuclei and cytoplasm occurred during spermiogenesis. In conjunction with the aforementioned structural abnormalities, sperm motility decreased and the path velocity of motile sperm was reduced (Fig. 5G).

We also examined sperm morphogenesis in the testes of *mgcl-1*$^{-/-}$ mice. In the testes, male germ cells differentiate from spermatogonia into sperm by the complex process of spermatogenesis (33). The murine spermatogenic cycle is well defined and can be subdivided into 12 stages (stages I to XII), with each stage consisting of a specific complement of male germ cells. The whole process of spermatogenesis occurs in three phases: spermatocytogenesis, meiosis, and spermiogenesis. In spermiogenesis, the spermatids undergo remarkable cytological transformations to develop from round spermatids to mature sperm (steps 1 to 16), via sequential differentiation through elongating spermatids and elongated spermatids. The dramatic morphological alterations of nuclei take place in both elongating and elongated spermatids. The disruption of nuclear structures was observed in elongating spermatids at step 9 in mutant mice. The cytoplasm was invaginated into elongating nuclei, which were frequently accompanied by bundles of microtubules (Fig. 6B). The invaginated cytoplasm was retained until the sperm developed (Fig. 5F). In addition, extrusion of the nucleoplasm from the condensed nucleus was observed in step 15 spermatids (Fig. 6C).

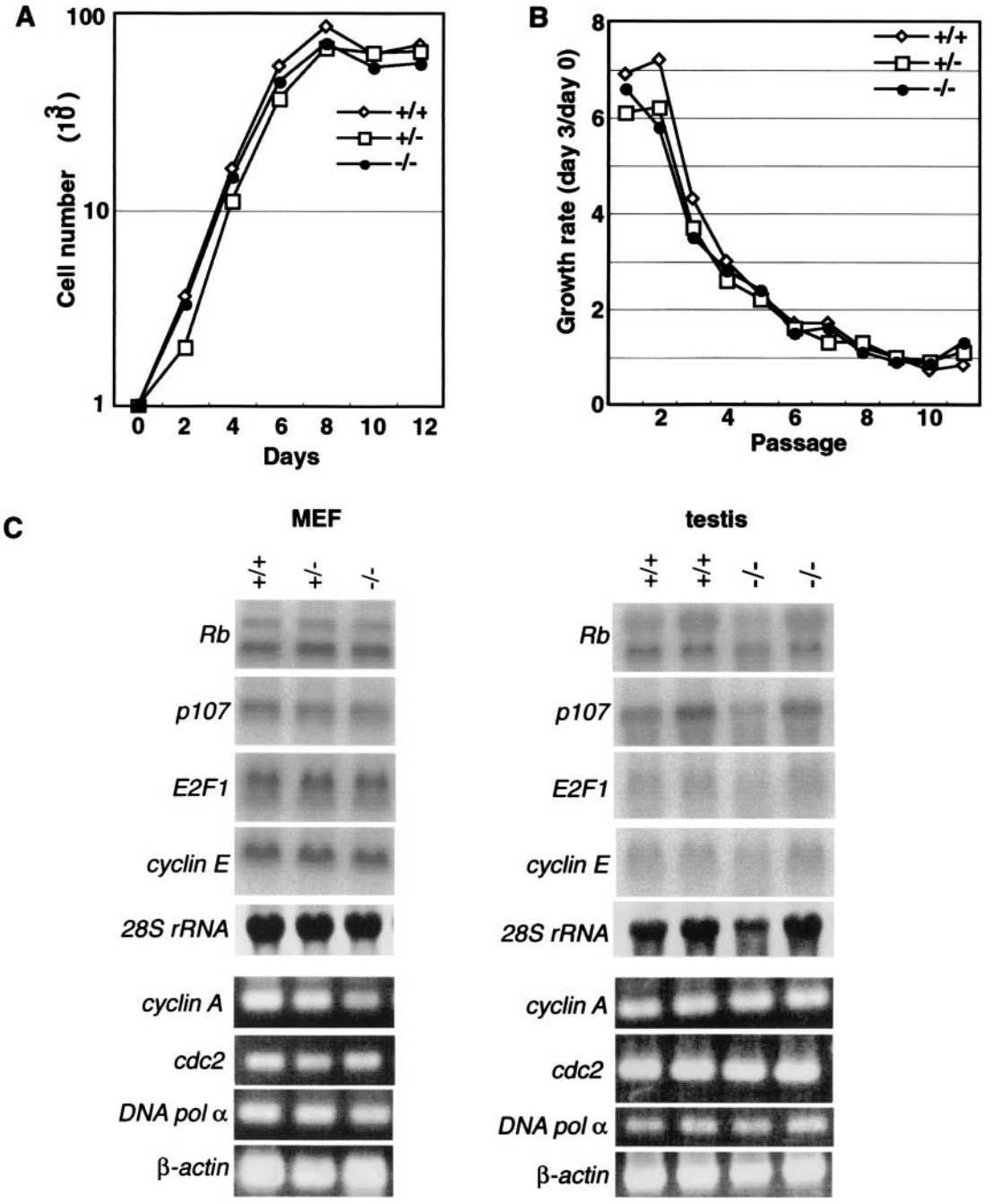

FIG. 2. Normal cell growth and E2F-DP target gene expression. (A) Growth rates and saturation densities of MEFs. Primary MEFs were seeded at 10^3 cells/well at day 0, and cells were counted every other day. (B) 3T3 analysis. MEF cultures were passaged according to the 3T3 protocol, and the growth rate was calculated as described in the Materials and Methods section. (C) Expression of the E2F target genes in MEFs and testes. Total RNA was extracted and subjected to Northern blotting or semiquantitative RT-PCR analysis.

The final step of spermiogenesis, i.e., spermiation, or the release of sperm from the seminiferous epithelium, occurs in step 16 spermatids (33, 42). In *mgcl-1*$^{-/-}$ mice, numerous multinucleated cells were present in the luminal side of the seminiferous epithelium in stage VIII tubules, but not in tubules at earlier stages (Fig. 6E and F). In addition, incomplete separation of nuclei from the cytoplasm and widening of the intercellular bridges was observed in step 16 spermatids of *mgcl-1*$^{-/-}$ mice (Fig. 6H and I). These observations strongly suggest that the premature release of syncytial spermatids that coalesce through the opening of bridges results in the formation of multinucleated, giant sperm with multiple heads and flagella.

Nuclear envelope proteins have been reported to redistribute during the process of spermatid elongation (4, 10). Immunohistochemical analysis with anti-NPC antibody showed that

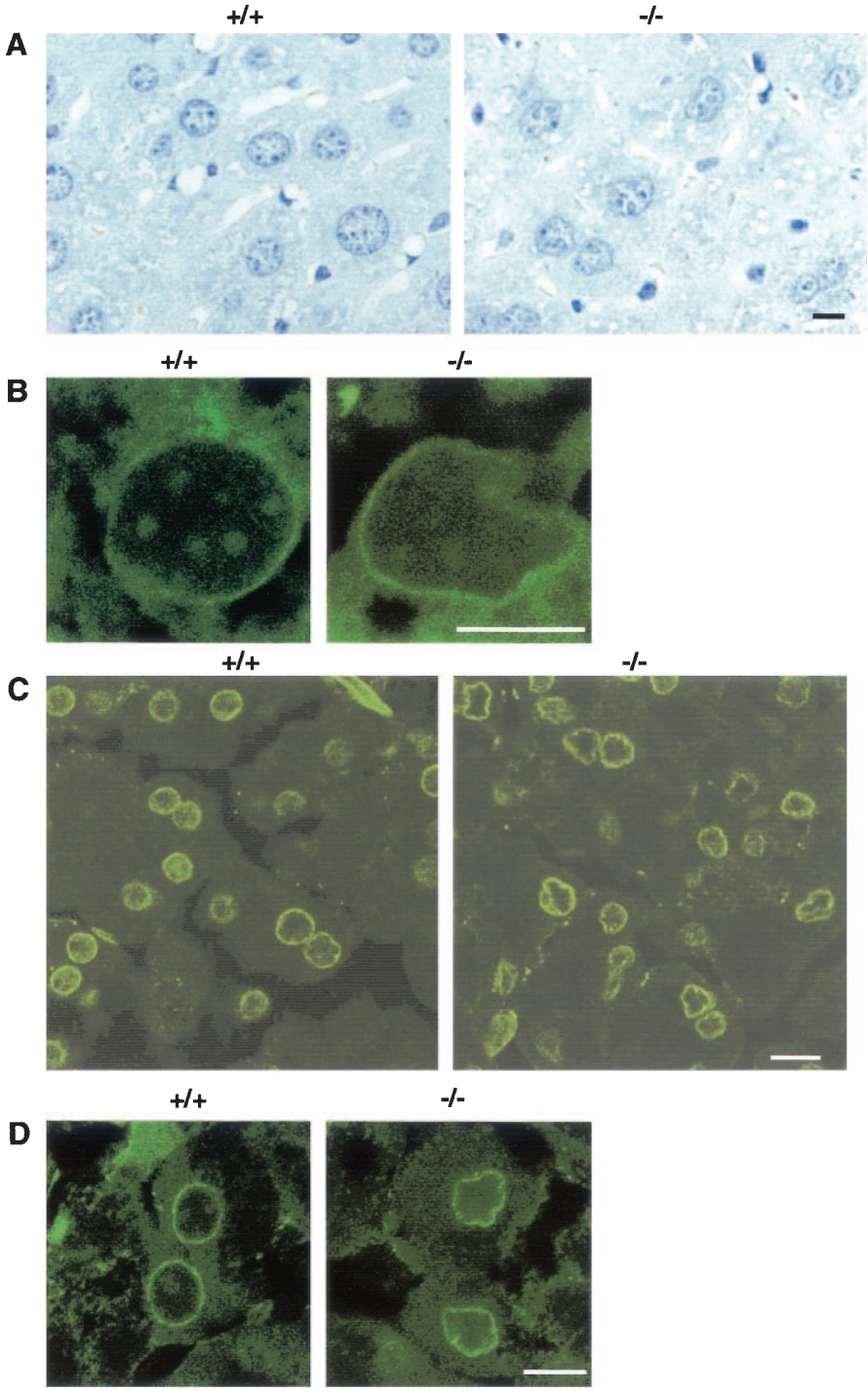

FIG. 3. Abnormal nuclear morphology in cells of the liver and exocrine pancreas of *mgcl-1*$^{-/-}$ mice. (A) Liver sections fixed with 4% paraformaldehyde. The nuclei were stained with hematoxylin. Liver sections that were fixed in Carnoy's solution showed the same abnormalities. (B) Liver sections stained with the anti-NPC antibody. (C and D) Pancreas sections stained with the anti-lamin B antibody. (B to D) Sections were analyzed using a confocal laser scanning microscope with 0.7-μm-thick optical sections. Scale bars, 10 μm.

NPC were concentrated at the posterior end of nucleus in elongating spermatids of *mgcl-1*$^{-/-}$ mice as well as in those of wild-type spermatids (data not shown), indicating that the redistribution of nuclear envelope proteins occurred normally even in the absence of mGCL-1.

Abnormal expression of chromatin-remodeling proteins during *mgcl-1*-null spermatogenesis. Chromatin remodeling is an essential part of spermatogenesis (16, 34). The sequential exchange of chromatin proteins from histones to protamines (Prm-1 and Prm-2) via transition proteins (TP-1 and TP-2) is

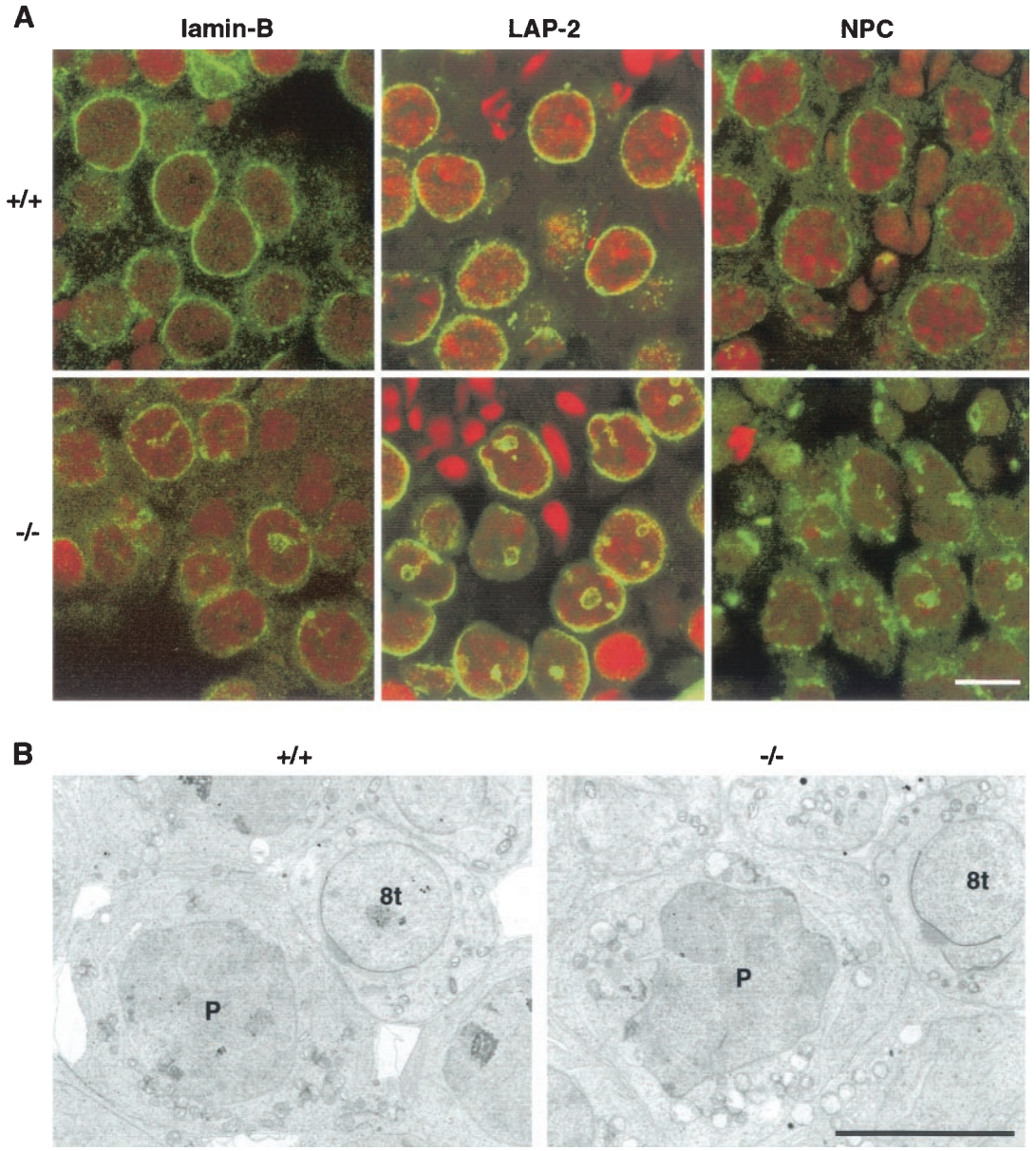

FIG. 4. Abnormal nuclear organization of spermatocytes in *mgcl-1*$^{-/-}$ mice. (A) The testis sections of wild-type and *mgcl-1*$^{-/-}$ mice were stained with antibodies against lamin B, LAP2, and NPC, and 1.0-μm-thick optical sections were analyzed by confocal microscopy. The sections were counterstained with propidium iodide, and the merged images are shown. Scale bar, 5 μm. (B) Electron micrographs of pachytene spermatocytes of wild-type and *mgcl-1*$^{-/-}$ mice. P, pachytene spermatocyte; 8t, step 8 spermatid. Scale bar, 5 μm.

accompanied by morphological changes in the nuclei and precipitates chromatin condensation in sperm heads (1, 9, 47, 49). Prm-1 is synthesized in its mature form, and Prm-2 is produced in a precursor form that is cleaved proteolytically. Although no significant differences were observed in the *Prm-1* and *Prm-2* mRNA levels of *mgcl-1*$^{+/+}$ and *mgcl-1*$^{-/-}$ testes (Fig. 7A), abnormalities were found in the protamines and transition proteins of *mgcl-1*$^{-/-}$ testes.

Protamines were extracted from equal numbers of sperm heads and subjected to acid urea polyacrylamide gel electrophoresis and Western blotting (Fig. 7B). The levels of Prm-1 and Prm-2 in the sperm of *mgcl-1*$^{-/-}$ mice were lower than those in the control mice. In addition, the immature precursor form of Prm-2 accumulated in the sperm of *mgcl-1*$^{-/-}$ mice. Immunohistochemical analyses of the testes indicated that translational activation of *Prm-1* and *Prm-2* occurred at the appropriate differentiation stages in spermatids (data not shown). Bearing in mind that the mRNA expression was normal, we conclude that abnormal posttranscriptional control of protamines took place in the *mgcl-1*$^{-/-}$ mice. However, we observed normal expression of three genes that are essential for posttranscriptional modifications of protamines, double-stranded RNA-binding protein Prbp (encoded by the gene *Tarbp2*), Ca^{2+}/calmodulin-dependent protein kinase IV (*Camk4*), and casein kinase II α′ isoform (*Csnk2a2*) (Fig. 7A) (44, 46, 51). Meanwhile, retention of the transition protein

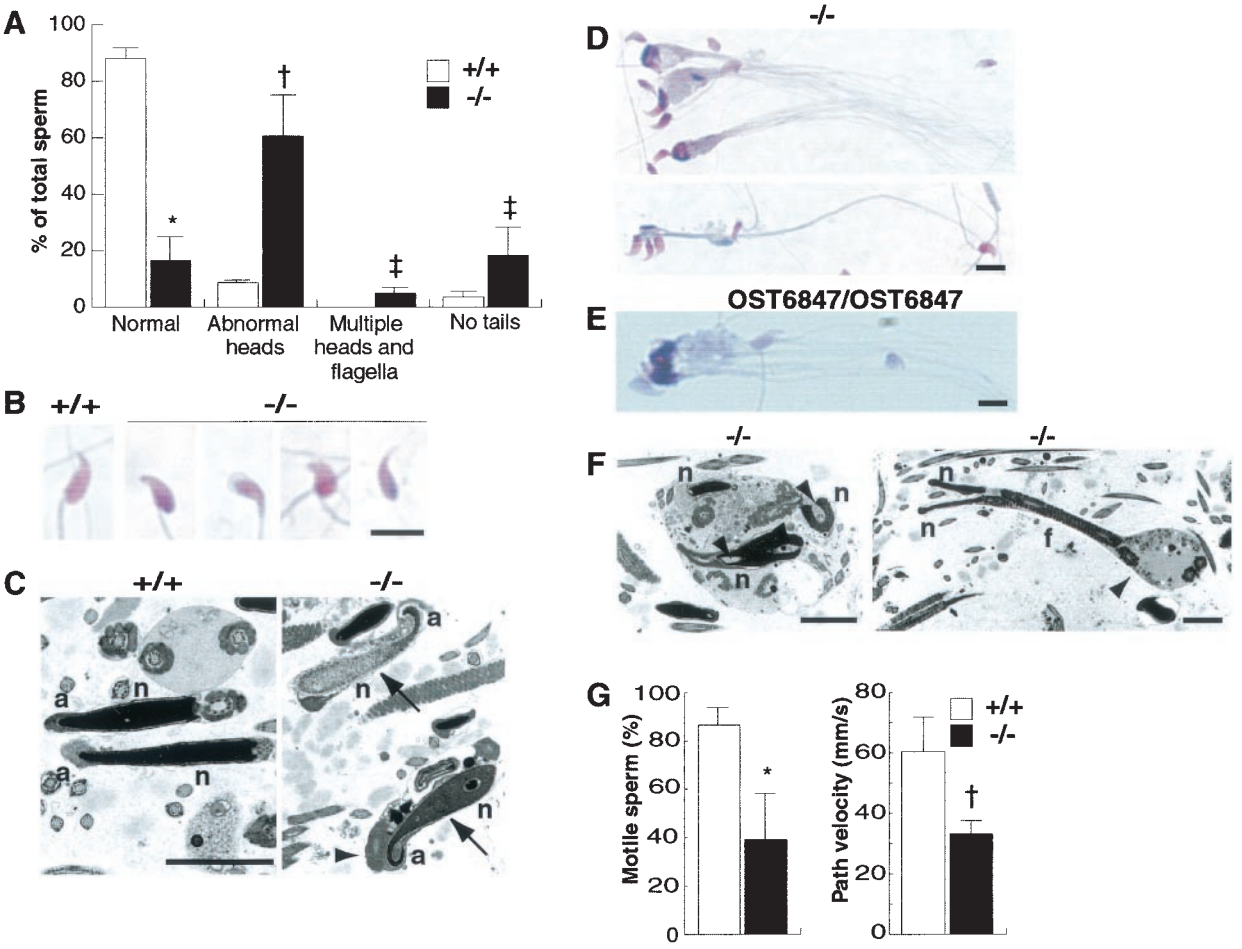

FIG. 5. Morphological and functional abnormalities in the sperm of *mgcl-1*$^{-/-}$ mice. (A) Sperm from the cauda epididymis of wild-type and *mgcl-1*$^{-/-}$ mice were stained with HE, and their morphology was classified into four categories (see text). Data are means (error bars, standard deviations) of results for four mice (symbols for statistical significance [Student's *t* test]: *, $P < 0.00001$; †, $P < 0.005$; ‡, $P < 0.05$). (B) Morphology of sperm heads. Typical abnormalities observed in *mgcl-1*$^{-/-}$ mice included blunt acrosomes, ectopic attachment of flagella, round heads, and narrowed heads (from left to right in the −/− panel). The sperm nuclei of *mgcl-1*$^{-/-}$ mice are relatively well stained with hematoxylin, which suggests incomplete condensation. Scale bar, 10 μm. (C) Electron micrographs of sperm heads. Electron-dense and highly condensed nuclei are observed in the wild-type mice, whereas nuclear condensation is incomplete in the *mgcl-1*$^{-/-}$ mice (arrows). The acrosomes of the sperm of *mgcl-1*$^{-/-}$ mice are curled. The cytoplasmic components, such as mitochondria, are retained in an abnormal fashion around the acrosome (arrowhead). Abbreviations; a, acrosome; f, flagellum; n, nucleus. Scale bar, 5 μm. (D and E) Giant sperm with multiple heads and flagella in *mgcl-1*$^{-/-}$ (D) and *mgcl-1*$^{OST4876/OST4876}$ (E) mice. Scale bars, 10 μm. (F) Electron micrographs of giant sperm in *mgcl-1*$^{-/-}$ mice. Three nuclei are embedded in a large section of the cytoplasm (left), and the cytoplasm is retained in the middle portion of the flagellum with two heads (right, arrowhead). Note the invaginated cytoplasm that is retained within the nuclei (left, arrowhead). Scale bar, 5 μm. (G) The percentage of motile sperm and the path velocity of motile sperm. Data represent the means (error bars, standard deviations) of four wild-type and six *mgcl-1*$^{-/-}$ mice (symbols for statistical significance [Student's *t* test]: *, $P < 0.005$; †, $P < 0.05$).

TP-2 was prolonged until the final stage of elongated spermatids in *mgcl-1*$^{-/-}$ testes (Fig. 7C).

DISCUSSION

mGCL-1 and nuclear integrity. The nuclear envelope, which separates the chromosomes from the cytoplasm and organizes the nuclear architecture, is composed of inner and outer membranes, NPC, and nuclear lamina (21, 43). The inner nuclear membrane contains a unique set of integral membrane proteins, which includes the lamin B receptor (LBR), LAP1, LAP2, emerin, MAN1, and nurim. Most of these proteins bind to the nuclear lamina, which is a network of polymers formed by lamins. Mammals have three lamin genes (*LMNA*, *LMNB*, and *LMNB2*), which encode seven alternatively spliced lamin isoforms. Lamins and other nuclear envelope proteins are involved in the organization of the nuclear architecture. From the analyses of human diseases and gene targeting mouse, three genes, *LMNA*, *emerin* and *LBR* have been revealed to be essential for the maintenance of normal nuclear envelope integrity as discussed later (21, 23).

The cells of *mgcl-1*-null mice showed abnormal nuclear structures in several organs (Fig. 3 and 4). Although mGCL-1 was reported to bind LAP2β, the functions of these two proteins in nuclear envelope formation remain unknown (14, 31). LBR and emerin are integral proteins of the nuclear inner

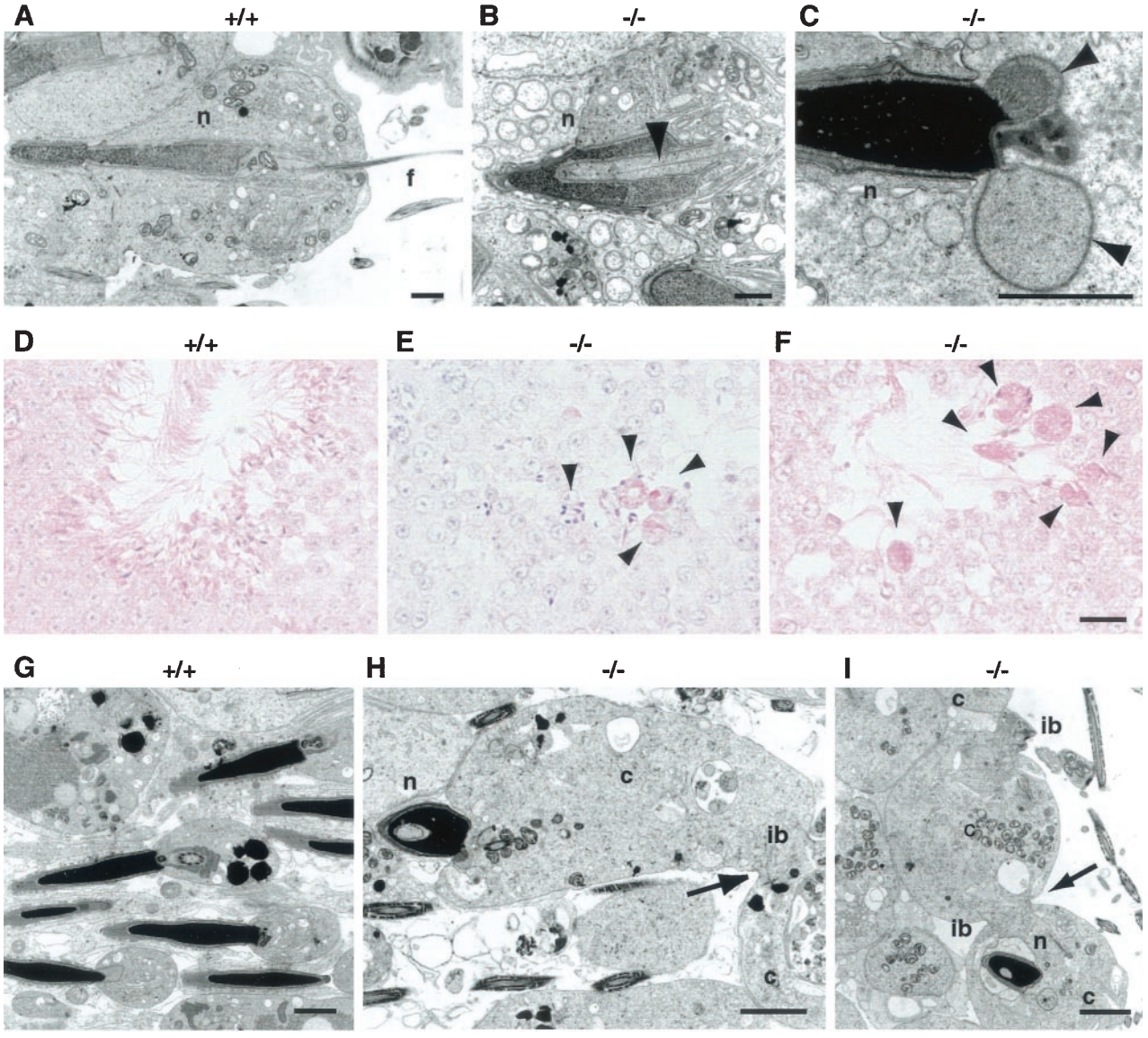

FIG. 6. Abnormal spermiogenesis in *mgcl-1*$^{-/-}$ mice. Shown are electron (A to C and G to I) and light (D to F) micrographs of adult testes. (A and B) Step 10 spermatids of wild-type (A) and *mgcl-1*$^{-/-}$ (B) mice. The arrowhead indicates the invaginated cytoplasm that accompanies the bundles of microtubules. (C) Step 15 spermatid of *mgcl-1*$^{-/-}$ mice. Arrowheads indicate nucleoplasm extrusions from the condensed nucleus. (A to C) Scale bars, 2 μm. (D to F) The stage VIII tubules of wild-type (D) and *mgcl-1*$^{-/-}$ (E and F) mice. Arrowheads indicate multinucleated cells. Scale bar, 20 μm. (G to I) Step 16 spermatids during spermiation in the wild-type (G) and *mgcl-1*$^{-/-}$ (H and I) mice. Incomplete separation of the nucleus from the cytoplasm (H), and nuclear embedding in the cytoplasm (I) are frequently observed in *mgcl-1*$^{-/-}$ mice. Arrows indicate the widening of intercellular bridges. Abbreviations: n, nucleus; f, flagellum; c, cytoplasm; ib, intercellular bridge. Scale bars, 2 μm.

membrane, and lamins A and C, which are A-type lamins and gene products of the *LMNA* gene, are major components of the nuclear lamin. Compared to these proteins, mGCL-1 appears to be a relatively minor component of the nuclear lamina, since mGCL-1 does not bind directly to lamins and it is not an integral protein (31). An essential role for mGCL1 in nuclear integrity suggests that the nuclear lamina forms a more complicated structure than was previously believed; i.e., more proteins may participate as essential members. An alternative, though not mutually exclusive, interpretation is that the *Drosophila* GCL and mGCL-1 proteins have unidentified molecular properties in common. Although there are no genes that code for LAP proteins in *Drosophila* (11), GCL is localized to the nuclear envelope (24, 32). Furthermore, mGCL-1 can rescue the *Drosophila gcl* mutant phenotype (29). In addition, the full-length mGCL-1 and various deletion mutants of mGCL-1 have been localized to the nuclear lamina (data not shown). It is conceivable that mGCL-1 binds to some other structural components of the nuclear envelope in order to maintain the structure.

Nuclear envelopes break down at the onset of mitosis and are reconstructed around the chromosomes during telophase (8, 12). Similar to other nuclear lamina proteins, mGCL-1 diffuses into cytoplasm and/or ER during mitosis and reassem-

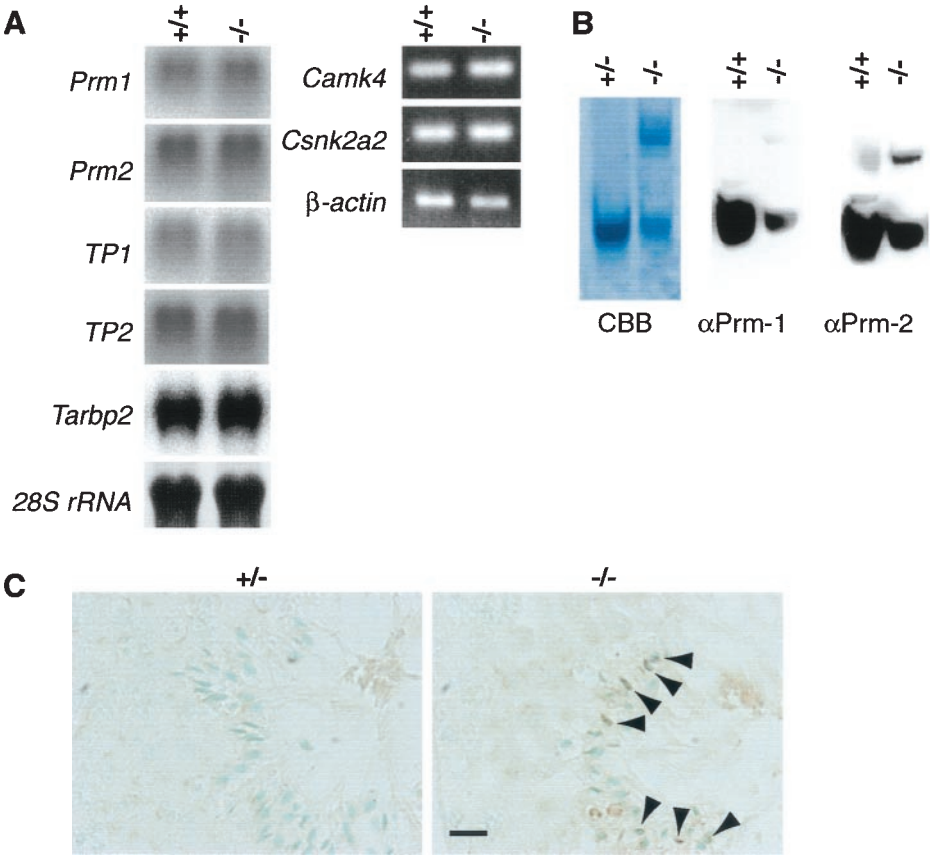

FIG. 7. Abnormal chromatin-remodeling proteins in *mgcl-1*$^{-/-}$ mice. (A) The expression of mRNAs for Prms, TPs, Tarbp2, Camk4, and Csnk2a2 was examined by Northern blotting or RT-PCR analysis. (B) Prms from the sperm of wild-type and *mgcl-1*$^{-/-}$ mice were separated on an acid urea polyacrylamide gel and either stained with Coomassie brilliant blue (CBB) or subjected to Western blot analysis with antibodies to Prm-1 (αPrm-1) or Prm-2 (αPrm-2). Protein from the same number of sperm was loaded in each lane. The top bands in the CBB-stained gels are precursor forms of Prm-2, and the lower band is a mixture of Prm-1 and Prm-2. (C) Immunohistochemical analysis of TP-2 in the testes of *mgcl-1*$^{+/-}$ and *mgcl-1*$^{-/-}$ mice. TP-2 was retained in an abnormal manner in late spermatids of *mgcl-1*$^{-/-}$ mice at stage VIII (arrowheads). Nuclei are counterstained with methyl green. Scale bar, 10 μm.

bles around chromosomes at the end of mitosis (data not shown). Immunostaining with antibodies against LAP2 and NPC showed that the nuclear envelope components assembled around chromosomes at the end of mitosis in *mgcl-1*$^{-/-}$ embryonic fibroblasts (data not shown), suggesting that reformation of nuclear envelopes was not affected by the absence of mGCL-1.

Abnormal spermatogenesis in *mgcl-1*$^{-/-}$ mice. The most striking feature of the *mgcl-1*$^{-/-}$ mouse phenotype was abnormal spermatogenesis (Fig. 4 to 7). The abnormalities could be divided into three categories: defects in nuclear architecture, sperm morphology, and proteins that were involved in chromatin remodeling. Given that mGCL-1 bound directly to LAP2β, and that mGCL-1 is expressed abundantly in spermatocytes (27, 29, 31), the abnormal nuclear envelope structure was probably due to the primary effect of the null mutation in *mgcl-1*. However, it is uncertain whether the other abnormalities are direct sequels of the null mutation or are due to the indirect effects of the abnormal nuclear envelope structure.

Although the *mgcl-1* gene was expressed ubiquitously, abnormal nuclear morphology was detected only in the restricted organs. The testes showed very high levels of *mgcl-1* mRNA. However, the mRNA levels in the exocrine pancreas and liver, both of which showed abnormal nuclear structures, were comparable to those in other organs (27, 29). Thus, the abundance of *mgcl-1* transcripts alone does not explain why mGCL-1 is important for the normal nuclear structure. Differential expression of lamins may be one reason for the tissue-specific nuclear architecture abnormalities. The nuclear envelope of spermatocytes contains the short meiosis-specific lamin isoforms C2 and B3, which are A- and B-type lamins, respectively (19, 20, 36, 41). Due to the presence of these spermatocyte-specific lamins, the stability of the nuclear envelope of spermatocytes is considered to be lower than that of somatic cells (3, 5, 19). Abnormal nuclear morphology was found not only in spermatocytes but also in the later stages of spermiogenesis. It seems reasonable to consider that the vulnerable nuclear structure originates in spermatocytes and persists until the later phases of spermatogenesis.

Experimental and genetic studies suggest that the nuclear lamina is involved in a number of nuclear functions, such as nuclear envelope assembly, DNA synthesis, transcription, and apoptosis (21, 43). The roles of the nuclear lamina in replica-

tion and transcription are putatively related to interactions between the nuclear lamina and chromatin. From this point of view, an intriguing phenotype of the *mgcl-1*-null mouse was the abnormal expression of transition proteins and protamines (Fig. 7), both of which are involved in chromatin remodeling during spermatogenesis (16, 34). It is unclear whether this abnormality is a direct consequence or an indirect downstream effect of nuclear envelope abnormality. In any case, this abnormality led to insufficient chromatin condensation in the sperm heads of *mgcl-1*$^{-/-}$ mice. Perturbed chromatin remodeling caused by the impaired expression of transition proteins and protamines may be one of the reasons why mature *mgcl-1*mutant sperm have abnormal morphologies (1, 9, 47, 49, 51).

Two previous works have suggested that mGCL-1 interferes with the transcriptional functions of the E2F-DP complex (13, 31). An independent explanation for the abnormality in *mgcl-1*$^{-/-}$ testis is that abnormal gene expression arose from the altered transcriptional activities of E2F-DP. However, we believe that this mechanism is unlikely to be true, since the expression levels of genes whose transcription was driven by E2F-DP were not altered significantly in the *mgcl-1*$^{-/-}$ testis (Fig. 2).

mGCL-1 as a factor of "laminopathies." Interestingly, perturbation of the nuclear envelope structure is known to cause laminopathy diseases, such as Emery-Dreifuss muscular dystrophy, in which the lamin A/C or the emerin genes for nuclear-lamina components are mutated (21, 43). Mice that lacked the A-type lamins had abnormal nuclear envelope integrity and suffered from muscular dystrophy (38). Recently, mutations in the LBR-encoding gene were reported to alter the nuclear morphology of granulocytes (Pelger-Huët anomaly) (23). These laminopathies are defined as diseases that are caused by mutations in genes that encode either lamins or proteins that bind to lamins. The loss of mGCL-1 may not in itself constitute a laminopathy, since mGCL-1 does not bind directly to lamins. However, mGCL-1 deficiency may be considered a laminopathy in a broader interpretation of this disease. In terms of both the human diseases and the mutant mouse strains, it has been proposed that defects in the nuclear lamina eliminate the specific interaction between the nuclear matrix and chromatin, which leads to disorganized chromatin architectures and abnormal gene expression. However, the molecular mechanisms that link abnormal nuclear envelope integrity and these diseases have not been elucidated (21, 43). It remains to be determined whether the pathophysiology reflects the primary molecular defect in the nuclear envelope, or is caused by downstream effects on chromatin structure and gene expression.

Accordingly, it is difficult to ascertain how the *mgcl-1*-null mutation causes abnormal spermatogenesis. However, we speculate that the LAP2-BAF association may provide a clue to the pathogenesis. Chromatin regions appear to be anchored to the nuclear lamina (21), and LAP2 is an important component for this binding, since two isoforms of LAP2, LAP2α and LAP2β, bind to chromatin (15, 18). Stable binding requires both the chromatin-binding domain and the LEM domain, which is a conserved region of ~43 amino acids that is also found in emerin and MAN1 (30, 35). In addition, LAP2 isoforms bind to the DNA-binding protein BAF via their LEM domains (17, 35). BAF, which is a ubiquitous and highly conserved protein, colocalizes with chromatin during interphase and mitosis and probably plays a fundamental role in chromosome architecture (17, 50). A null mutation in the *mgcl-1* gene may affect chromatin organization and subsequent gene expression by inducing an abnormal LAP2β-BAF association.

The *Drosophila gcl* gene is required for the formation of germ cell precursors but not for germ cell development within the gonads (25, 32). In contrast, *mgcl-1* is dispensable for PGC formation (data not shown) but is important for spermatogenesis. Thus, despite the substitutable molecular function of mouse *gcl* in *Drosophila*, the physiological functions of the *Drosophila* and mouse *gcl* genes are distinct during germ cell development. One of the abnormal features of the *Drosophila gcl* mutant is the disordered budding of germ lineage cells (25, 32). The gigantic sperm in *mgcl-1*$^{-/-}$ mice, which were presumably caused by unsuccessful cell separation at the final stage of spermiogenesis, are reminiscent of abnormal budding in *Drosophila*. We believe that comparative studies in different taxa of the functions of the *Drosophila* GCL and its mouse homologue will provide phylogenetic clues as to germ cell specification and differentiation.

ACKNOWLEDGMENTS

We thank R. Balhorn, S. Kestler, J. Takeda, and Y. Yoneda for providing antibodies and plasmids and A. Mizokami and Y. Maruyama for assistance.

This work was supported in part by grants from the Ministry of Education, Science, Sports, and Culture; Japanese Society for Promotion of Science (JSPS-RFTF98L01101); Yamanouchi Foundation for Research on Metabolic Disorders; Osaka Cancer Foundation; and Osaka Cancer Research Foundation.

REFERENCES

1. **Adham, I. M., K. Nayernia, E. Burkhardt-Gottges, O. Topaloglu, C. Dixkens, A. F. Holstein, and W. Engel.** 2001. Teratozoospermia in mice lacking the transition protein 2 (Tnp2). Mol. Hum. Reprod. **7:**513–520.
2. **Alfonso, P. J., and W. S. Kistler.** 1993. Immunohistochemical localization of spermatid nuclear transition protein 2 in the testes of rats and mice. Biol. Reprod. **48:**522–529.
3. **Alsheimer, M., and R. Benavente.** 1996. Change of karyoskeleton during mammalian spermatogenesis: expression pattern of nuclear lamin C2 and its regulation. Exp. Cell Res. **228:**181–188.
4. **Alsheimer, M., E. Fecher, and R. Benavente.** 1998. Nuclear envelope remodelling during rat spermiogenesis: distribution and expression pattern of LAP2/thymopopietins. J. Cell Sci. **111:**2227–2234.
5. **Alsheimer, M., E. von Glasenapp, R. Hock, and R. Benavente.** 1999. Architecture of the nuclear periphery of rat pachytene spermatocytes: distribution of nuclear envelope proteins in relation to synaptonemal complex attachment sites. Mol. Biol. Cell **10:**1235–1245.
6. **Balhorn, R., B. L. Gledhill, and A. J. Wyrobek.** 1977. Mouse sperm chromatin proteins: quantitative isolation and partial characterization. Biochemistry **16:**4074–4080.
7. **Bardwell, V. J., and R. Treisman.** 1994. The POZ domain: a conserved protein-protein interaction motif. Genes Dev. **8:**1664–1677.
8. **Buendia, B., J. C. Courvalin, and P. Collas.** 2001. Dynamics of the nuclear envelope at mitosis and during apoptosis. Cell. Mol. Life Sci. **58:**1781–1789.
9. **Cho, C., W. D. Willis, E. H. Goulding, H. Jung-Ha, Y. C. Choi, N. B. Hecht, and E. M. Eddy.** 2001. Haploinsufficiency of protamine-1 or -2 causes infertility in mice. Nat. Genet. **28:**82–86.
10. **Clermont, Y., R. Oko, and L. Hermo.** 1993. Cell biology of mammalian spermiogenesis, p. 332–376. *In* C. Desjardins and L. L. Ewing (ed.), Cell and molecular biology of the testis. Oxford Press: New York, N.Y.
11. **Cohen, M., K. K. Lee, K. L. Wilson, and Y. Gruenbaum.** 2001. Transcriptional repression, apoptosis, human disease and the functional evolution of the nuclear lamina. Trends Biochem. Sci. **26:**41–47.
12. **Collas, I., and J. C. Courvalin.** 2000. Sorting nuclear membrane proteins at mitosis. Trends Cell Biol. **10:**5–8.
13. **Dechat, T., S. Vlcek, and R. Foisner.** 2000. Lamina-associated polypeptide 2 isoforms and related proteins in cell cycle-dependent nuclear structure dynamics. J. Struct. Biol. **129:**335–345.
14. **de la Luna, S., K. E. Allen, S. L. Mason, and N. B. La Thangue.** 1999. Integration of a growth-suppressing BTB/POZ domain protein with the DP component of the E2F transcription factor. EMBO J. **18:**212–228.

15. **Foisner, R., and L. Gerace.** 1993. Integral membrane proteins of the nuclear envelope interact with lamins and chromosomes, and binding is modulated by mitotic phosphorylation. Cell **73:**1267–1279.
16. **Fuentes-Mascorro, G., H. Serrano, and A. Rosado.** 2000. Sperm chromatin. Arch. Androl. **45:**215–225.
17. **Furukawa, K.** 1999. LAP2 binding protein 1 (L2BP1/BAF) is a candidate mediator of LAP2-chromatin interaction. J. Cell Sci. **112:**2485–2492.
18. **Furukawa, K., C. Glass, and T. Kondo.** 1997. Characterization of the chromatin binding activity of lamina-associated polypeptide (LAP) 2. Biochem. Biophys. Res. Commun. **238:**240–246.
19. **Furukawa, K., and Y. Hotta.** 1993. cDNA cloning of a germ cell specific lamin B3 from mouse spermatocytes and analysis of its function by ectopic expression in somatic cells. EMBO J. **12:**97–106.
20. **Furukawa, K., H. Inagaki, and Y. Hotta.** 1994. Identification and cloning of an mRNA coding for a germ cell-specific A-type lamin in mice. Exp. Cell Res. **212:**426–430.
21. **Goldman, R. D., Y. Gruenbaum, R. D. Moir, D. K. Shumaker, and T. P. Spann.** 2002. Nuclear lamins: building blocks of nuclear architecture. Genes Dev. **16:**533–547.
22. **Heidaran, M. A., R. M. Showman, and W. S. Kistler.** 1988. A cytochemical study of the transcriptional and translational regulation of nuclear transition protein 1 (TP1), a major chromosomal protein of mammalian spermatids. J. Cell Biol. **106:**1427–1433.
23. **Hoffmann, K., C. K. Dreger, A. L. Olins, D. E. Olins, L. D. Shultz, B. Lucke, H. Karl, R. Kaps, D. Muller, A. Vaya, J. Aznar, R. E. Ware, N. S. Cruz, T. H. Lindner, H. Herrmann, A. Reis, and K. Sperling.** 2002. Mutations in the gene encoding the lamin B receptor produce an altered nuclear morphology in granulocytes (Pelger Huet anomaly). Nat. Genet. **31:**410–414.
24. **Jongens, T. A., L. D. Ackerman, J. R. Swedlow, L. Y. Jan, and Y. N. Jan.** 1994. Germ cell-less encodes a cell type-specific nuclear pore-associated protein and functions early in the germ-cell specification pathway of Drosophila. Genes Dev. **8:**2123–2136.
25. **Jongens, T. A., B. Hay, L. Y. Jan, and Y. N. Jan.** 1992. The germ cell-less gene product: a posteriorly localized component necessary for germ cell development in Drosophila. Cell **70:**569–584.
26. **Kimura, T., K. Nakayama, J. Penninger, M. Kitagawa, H. Harada, T. Matsuyama, N. Tanaka, R. Kamijo, J. Vilcek, T. W. Mak, and T. Taniguchi.** 1994. Involvement of the IRF-1 transcription factor in antiviral responses to interferons. Science **264:**1921–1924.
27. **Kimura, T., K. Yomogida, N. Iwai, Y. Kato, and T. Nakano.** 1999. Molecular cloning and genomic organization of mouse homologue of Drosophila germ cell-less and its expression in germ lineage cells. Biochem. Biophys. Res. Commun. **262:**223–230.
28. **Lavia, P., and P. Jansen-Durr.** 1999. E2F target genes and cell-cycle checkpoint control. Bioessays **21:**221–230.
29. **Leatherman, J. L., K. H. Kaestner, and T. A. Jongens.** 2000. Identification of a mouse germ cell-less homologue with conserved activity in Drosophila. Mech. Dev. **92:**145–153.
30. **Lin, F., D. L. Blake, I. Callebaut, I. S. Skerjanc, L. Holmer, M. W. McBurney, M. Paulin-Levasseur, and H. J. Worman.** 2000. MAN1, an inner nuclear membrane protein that shares the LEM domain with lamina-associated polypeptide 2 and emerin. J. Biol. Chem. **275:**4840–4847.
31. **Nili, E., G. S. Cojocaru, Y. Kalma, D. Ginsberg, N. G. Copeland, D. J. Gilbert, N. A. Jenkins, R. Berger, S. Shaklai, N. Amariglio, F. Brok-Simoni, A. J. Simon, and G. Rechavi.** 2001. Nuclear membrane protein LAP2beta mediates transcriptional repression alone and together with its binding partner GCL (germ-cell-less). J. Cell Sci. **114:**3297–3307.
32. **Robertson, S. E., T. C. Dockendorff, J. L. Leatherman, D. L. Faulkner, and T. A. Jongens.** 1999. germ cell-less is required only during the establishment of the germ cell lineage of Drosophila and has activities which are dependent and independent of its localization to the nuclear envelope. Dev. Biol. **215:**288–297.
33. **Russell, L. D., R. A. Ettlin, A. P. S. Hikim, and E. M. E. Clegg.** 1990. Histological and histopathological evaluation of the testis. Cache River Press, Clearwater, Fla.
34. **Sassone-Corsi, P.** 2002. Unique chromatin remodeling and transcriptional regulation in spermatogenesis. Science **296:**2176–2178.
35. **Shumaker, D. K., K. K. Lee, Y. C. Tanhehco, R. Craigie, and K. L. Wilson.** 2001. LAP2 binds to BAF · DNA complexes: requirement for the LEM domain and modulation by variable regions. EMBO J. **20:**1754–1764.
36. **Smith, A., and R. Benavente.** 1992. Identification of a short nuclear lamin protein selectively expressed during meiotic stages of rat spermatogenesis. Differentiation **52:**55–60.
37. **Stanker, L. H., A. Wyrobek, C. McKeown, and R. Balhorn.** 1993. Identification of the binding site of two monoclonal antibodies to human protamine. Mol. Immunol. **30:**1633–1638.
38. **Sullivan, T., D. Escalante-Alcalde, H. Bhatt, M. Anver, N. Bhat, K. Nagashima, C. L. Stewart, and B. Burke.** 1999. Loss of A-type lamin expression compromises nuclear envelope integrity leading to muscular dystrophy. J. Cell Biol. **147:**913–920.
39. **Todaro, G. J., and H. Green.** 1963. Quantitative studies of the growth of mouse embryo cells in culture and their development into established lines. J. Cell Biol **17:**299–313.
40. **Tybulewicz, V. L., C. E. Crawford, P. K. Jackson, R. T. Bronson, and R. C. Mulligan.** 1991. Neonatal lethality and lymphopenia in mice with a homozygous disruption of the c-abl proto-oncogene. Cell **65:**1153–1163.
41. **Vester, B., A. Smith, G. Krohne, and R. Benavente.** 1993. Presence of a nuclear lamina in pachytene spermatocytes of the rat. J. Cell Sci. **104:**557–563.
42. **Weber, J. E., and L. D. Russell.** 1987. A study of intercellular bridges during spermatogenesis in the rat. Am. J. Anat. **180:**1–24.
43. **Wilson, K. L., M. S. Zastrow, and K. K. Lee.** 2001. Lamins and disease: insights into nuclear infrastructure. Cell **104:**647–650.
44. **Wu, J. Y., T. J. Ribar, D. E. Cummings, K. A. Burton, G. S. McKnight, and A. R. Means.** 2000. Spermiogenesis and exchange of basic nuclear proteins are impaired in male germ cells lacking Camk4. Nat. Genet. **25:**448–452.
45. **Wylie, C.** 1999. Germ cells. Cell **96:**165–174.
46. **Xu, X., P. A. Toselli, L. D. Russell, and D. C. Seldin.** 1999. Globozoospermia in mice lacking the casein kinase II alpha' catalytic subunit. Nat. Genet. **23:**118–121.
47. **Yu, Y. E., Y. Zhang, E. Unni, C. R. Shirley, J. M. Deng, L. D. Russell, M. M. Weil, R. R. Behringer, and M. L. Meistrich.** 2000. Abnormal spermatogenesis and reduced fertility in transition nuclear protein 1-deficient mice. Proc. Natl. Acad. Sci. USA **97:**4683–4688.
48. **Zambrowicz, B. P., G. A. Friedrich, E. C. Buxton, S. L. Lilleberg, C. Person, and A. T. Sands.** 1998. Disruption and sequence identification of 2,000 genes in mouse embryonic stem cells. Nature **392:**608–611.
49. **Zhao, M., C. R. Shirley, Y. E. Yu, B. Mohapatra, Y. Zhang, E. Unni, J. M. Deng, N. A. Arango, N. H. Terry, M. M. Weil, L. D. Russell, R. R. Behringer, and M. L. Meistrich.** 2001. Targeted disruption of the transition protein 2 gene affects sperm chromatin structure and reduces fertility in mice. Mol. Cell Biol. **21:**7243–7255.
50. **Zheng, R., R. Ghirlando, M. S. Lee, K. Mizuuchi, M. Krause, and R. Craigie.** 2000. Barrier-to-autointegration factor (BAF) bridges DNA in a discrete, higher-order nucleoprotein complex. Proc. Natl. Acad. Sci. USA **97:**8997–9002.
51. **Zhong, J., A. H. Peters, K. Lee, and R. E. Braun.** 1999. A double-stranded RNA binding protein required for activation of repressed messages in mammalian germ cells. Nat. Genet. **22:**171–174.